Spray Pyrolysis Deposition and Photoelectrochemical Properties of n-Type BiOI Nanoplatelet Thin Films

Nathan T. Hahn, Son Hoang, Jeffrey L. Self, and C. Buddie Mullins*

Departments of Chemical Engineering and Chemistry and Biochemistry, Center for Electrochemistry, Texas Materials Institute, Center for Nano- and Molecular Science, The University of Texas at Austin C0400, 1 University Station, Austin, Texas 78712, United States

ABSTRACT

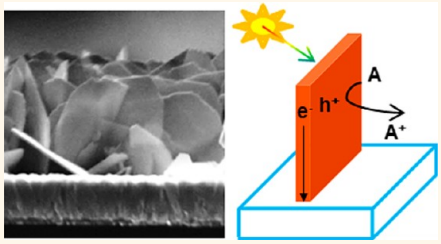

Bismuth oxy-iodide is a potentially interesting visible-light-active photocatalyst; yet there is little research regarding its photoelectrochemical properties. Herein we report the synthesis of BiOI nanoplatelet photoelectrodes by spray pyrolysis on fluorine-doped tin oxide substrates at various temperatures. The films exhibited n-type conductivity, most likely due to the presence of anion vacancies, and optimized films possessed incident photon conversion efficiencies of over 20% in the visible range for the oxidation of I^- to I_3^- at 0.4 V *vs* Ag/AgCl in acetonitrile. Visible-light photons ($\lambda > 420$ nm) contributed approximately 75% of the overall photocurrent under AM1.5G illumination, illustrating their usefulness under solar light illumination. A deposition temperature of 260 °C was found to result in the best performance due to the balance of morphology, crystallinity, impurity levels, and optical absorption, leading to photocurrents of roughly 0.9 mA/cm^2 at 0.4 V *vs* Ag/AgCl. Although the films performed stably in acetonitrile, their performance decreased significantly upon extended exposure to water, which was apparently caused by a loss of surface iodine and subsequent formation of an insulating bismuth hydroxide layer.

KEYWORDS: visible-light photocatalyst · solar energy · water splitting · layered semiconductor

Photocatalysis is an active area of research due to its application in renewable and sustainable efforts such as artificial photosynthesis and hazardous pollutant removal.[1,2] Classically, wide band gap materials such as TiO_2 (3.0−3.2 eV) have been employed extensively for these purposes at the laboratory scale,[3] but in order to achieve commercial viability, materials capable of absorbing and utilizing visible light ($420 < \lambda < 700$ nm), comprising nearly half of the terrestrial solar spectrum, must be developed. A particularly ambitious goal of photocatalyst research is the development of materials capable of acting as photoelectrodes for water splitting, the generation of molecular hydrogen and oxygen from water.[4] Although a great deal of work has been performed in this area, further research of promising candidate materials is needed if reasonable solar conversion efficiencies are to be realized in such a photoelectrochemical (PEC) system.

One such material that has seen a recent surge of interest in the field of photocatalysis is BiOI.[5−9] This layered oxy-halide compound is typically synthesized in solution by precipitation or solvothermal methods, leading to powders having a bright red color indicative of its excellent band gap for solar energy utilization (1.8−1.9 eV).[5,6] Several such studies have found BiOI powders to be superior photocatalysts for the degradation of water-borne organic contaminants compared to other bismuth oxy-halides or doped TiO_2.[7−9] The high photocatalytic activity of bismuth oxy-halides has been attributed to their superior charge separation and transfer as a result of their open, layered crystal structure and more dispersive band characteristics compared to those present in transition metal oxides such as TiO_2.[10] Heterojunction photocatalysts such as BiOI-TiO_2, BiOI-ZnO, and BiOI-AgI have also been studied for photocatalytic applications.[11−13] Thin films of BiOI have recently been synthesized by successive ionic layer adsorption and reaction for characterization in photoelectrochemical solar cells, although the observed photocurrent (0.24 mA/cm^2) and efficiency (0.09%) were somewhat low.[14]

One characteristic of such layered semiconductors is that they possess covalently bonded slabs that are joined together by van der Waals interactions. As a result, their

* Address correspondence to mullins@che.utexas.edu.

Received for review April 2, 2012 and accepted August 14, 2012.

Published online August 14, 2012
10.1021/nn3031063

single-crystal surfaces (formed at this so-called van der Waals face) do not have dangling bonds and are expected to be self-passivating, minimizing the influence of surface states and photocorrosion, making them particularly interesting for PEC applications.[15] Additionally, the positions of the band edges of BiOI appear to be favorable for photo-oxidizing a variety of possible solution species.[16] These characteristics provide significant motivation for the further study of BiOI thin film photoelectrodes. Although the earliest PEC studies on BiOI thin films demonstrated p-type behavior and poor PEC performance,[17] in this work we demonstrate the strong PEC performance of nanostructured films of *n*-type BiOI deposited by spray pyrolysis.

The Results and Discussion portion of this paper is composed of several sections describing our study and details regarding the various measurements conducted beginning with film synthesis and concluding with film behavior in aqueous electrolyte. Briefly, we find that the spray pyrolysis technique can be successfully employed to deposit BiOI nanoplatelet films that are photoelectrochemically active. The film deposition temperature affects the size of the nanoplatelets as well as their crystallinity, composition, morphology, and optical properties. A major finding of our study is that the deposited BiOI semiconducting films exhibit n-type conductivity in contrast to reports employing other deposition strategies. The assignment of n-type conductivity is supported by (i) the measurement of anodic currents in a PEC cell upon illumination and (ii) Mott−Schottky measurements, the plots of which exhibit a positive slope that decreases with deposition temperature, indicating a change in donor density qualitatively consistent with increased anion vacancy concentrations at higher deposition temperatures as suggested *via* EDX and XPS measurements. Regarding the PEC activity, we find that a deposition temperature of 260 °C yields films with the best PEC performance for the oxidation of I^- to I_3^- in acetonitrile (0.9 mA/cm^2 at 0.4 V *vs* Ag/AgCl under AM1.5G). Additionally, the films possess indirect band gaps ranging from 1.7 to 1.8 eV and respond well to visible light with ∼75% of the photocurrent resulting from the visible portion of the spectrum. Unfortunately, the films show poor stability in aqueous solutions due to the formation of a surface hydroxide layer that hinders hole transfer. However, protection of n-BiOI films *via* an electrocatalyst layer or utilizing the material in a buried heterojunction scheme may be profitable. Further details of the findings reported above follow immediately.

RESULTS AND DISCUSSION

Film Deposition. Spray pyrolysis deposition parameters such as temperature, concentration, and number of cycles were varied in order to manipulate our BiOI film properties. Of these parameters, deposition temperature had the most influence on film properties. A precursor solution of 0.02 M $Bi(NO_3)_3$ and 0.04 M NH_4I in ethylene glycol was sprayed onto the heated substrates held at various temperatures. The spray rate was adjusted accordingly to produce uniform films of similar thicknesses. Ethylene glycol was required as the solvent in order to prevent the premature reaction of Bi^{3+} with I^- and water to produce BiOI precipitate. Since the autoignition temperature of ethylene glycol (410 °C) is much higher than the substrate temperatures studied, it is unlikely that there would be any effects of ethylene glycol combustion during deposition. Both potassium iodide and elemental iodine were tried as iodide sources in the precursor solution, but the former resulted in a large potassium contamination in the films and the latter did not react to form BiOI under any of the attempted conditions (only Bi_2O_3 was formed).

Film Morphology. Scanning electron microscopy (SEM) images of films deposited between 225 and 300 °C using $Bi(NO_3)_3$ and NH_4I revealed a clear trend in size and shape with increasing deposition temperature (Figure 1a). In all cases nanoplatelets were observed, and these platelets grew larger and more square-shaped with increasing deposition temperature. At 225 °C uniform platelet coverage was not observed over the entire sample, suggesting that higher temperatures were necessary to consistently form platelets across the entire substrate. Profile SEM images indicated that the thicknesses of typical BiOI films were approximately 1 μm (Figure 1a). Nearly all previous studies on BiOI show platelet-type structures as well, although the platelets are typically aggregated into larger (1−5 μm diameter) particles rather than remaining stable as a uniformly distributed thin film.[5,18−20] These earlier studies also demonstrated that BiOI platelets typically grow within the (001) plane, meaning that the *c*-axis is normal to the platelet faces.[10,16,20] This results from the layered crystal structure of BiOI, which consists of nonbonding layers of [I−Bi−O−Bi−I] slabs stacked along the *c*-axis.[20,21] This structure suggests that the platelet faces would normally be terminated by iodine, although vacancies and/or substitution by other species appears to occur in some cases. Another major implication of this layered structure is that the electronic properties of BiOI are anisotropic, with better electronic conductivity within the (001) plane compared to along the [001] direction.

High-resolution transmission electron microscopy (HRTEM) analyses of films deposited at 260 and 275 °C indicated that the platelets did not consistently form as single crystals until 275 °C. The nanoplatelets deposited at 260 °C were not single-crystalline in all cases, but tended to show a preferred in-plane (010) orientation (perpendicular to the *b*-axis), whereas platelets deposited at 275 °C showed an in-plane (001) orientation (perpendicular to the *c*-axis) (Figure 1b, c). Due to

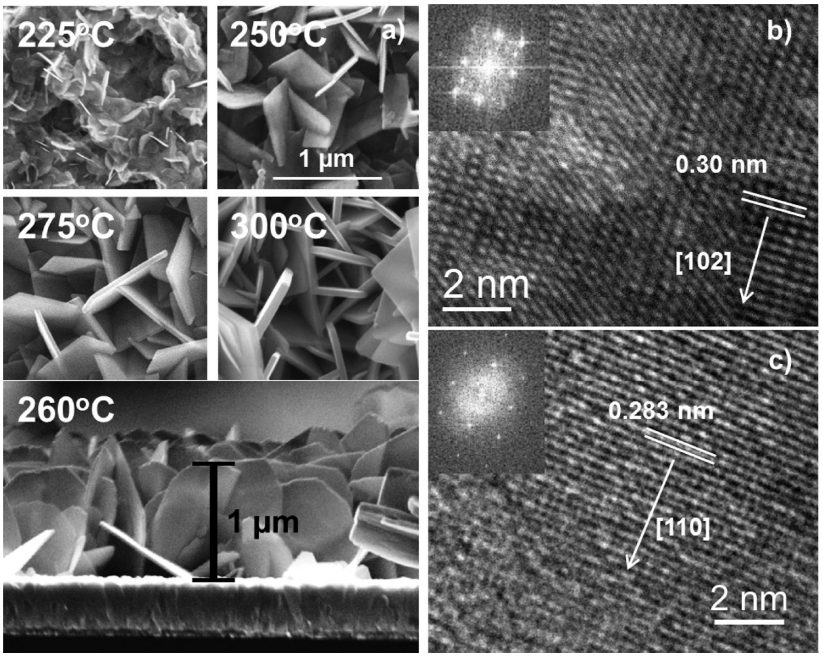

Figure 1. (a) SEM images of BiOI films deposited at the indicated temperatures on FTO-coated glass substrates. The scale bar of the 250 °C SEM image applies to the other top-view images as well. (b) HRTEM image and discrete-Fourier-transform (DFT) of a BiOI platelet deposited at 260 °C. (c) HRTEM image and DFT of a platelet deposited at 275 °C.

the layered structure of BiOI, one would expect the (001) orientation to be the preferred structure. Estimates of average platelet thicknesses measured from SEM images increased from 24 to 43 nm as the deposition temperature increased from 225 to 300 °C, respectively, although the standard deviations of the thicknesses measured in each film are 8−15 nm (Figure 2a). X-ray diffraction (XRD) patterns of films deposited over this temperature range also showed an increase in peak sharpness as the deposition temperature increased, signifying the growth of larger crystals (Figure 2b). All films showed polycrystalline patterns corresponding to tetragonal BiOI (powder diffraction file #01-075-5209), and in each case the preferred orientation overall was (102) followed by (110).

Film Composition. Preliminary energy dispersive X-ray spectroscopy (EDX) results indicated that a stoichiometric (1:1) ratio of iodine to bismuth in the precursor solution resulted in very I-deficient films. However, a 2:1 ratio of iodine to bismuth achieved only slight iodine deficiencies in films deposited between 225 and 300 °C (Figure 2c). Only at 325 °C was significant bulk iodine lost, presumably due to further oxidation of the films toward $Bi_4O_5I_2$, which we observed by XRD when BiOI powders were annealed to 350 °C. EDX analyses also showed that the films were deficient in oxygen, although the accuracy of this technique for the detection of such light elements is poor. BiOI powders produced by a low-temperature precipitation method also showed both oxygen and iodine deficiencies, indicating that anion vacancies may not be isolated to films deposited by spray pyrolysis alone and may occur in other BiOI materials also. To better understand the formation mechanism of BiOI, samples were deposited onto substrates held at lower temperatures and analyzed by XRD (see Supporting Information, Figure S-1). At a substrate temperature of 150 °C no crystalline phases were observed, but at 190 °C XRD peaks corresponding to BiI_3 were observed, indicating that the reaction of the dissolved precursor compounds to form BiOI likely proceeds *via* two steps:

$$Bi^{3+} + 3I^- = BiI_3 \quad (1)$$

$$BiI_3 + \frac{1}{2}O_2 = BiOI + I_2 \quad (2)$$

From X-ray photoelectron spectroscopy (XPS) analyses the average surface ratio of I:Bi was determined to be 0.74 ± 0.03 for the samples deposited between 250 and 300 °C, suggesting that surface iodine loss under exposure to the atmosphere at these temperatures may be unavoidable. A possible reason for this is the substitution of OH^- species for I^- on the surface of the films, based on the enhanced ratio of O:Bi measured by XPS (0.8 to 1.1) relative to the bulk values measured by EDX (~0.7). The O 1s spectrum measured by XPS for a film deposited at 260 °C is displayed in Figure 2d along with fitted component peaks located at 529.9, 531.4, and 532.9 eV. The lowest binding energy peak is typical of that observed for metal oxides, indicating that it should be assigned to lattice O in BiOI.[9,22] The other two fitted peaks are more difficult to assign, but likely represent surface-bound O-containing species such as OH and/or organic impurities.[9] The ratio of the lattice

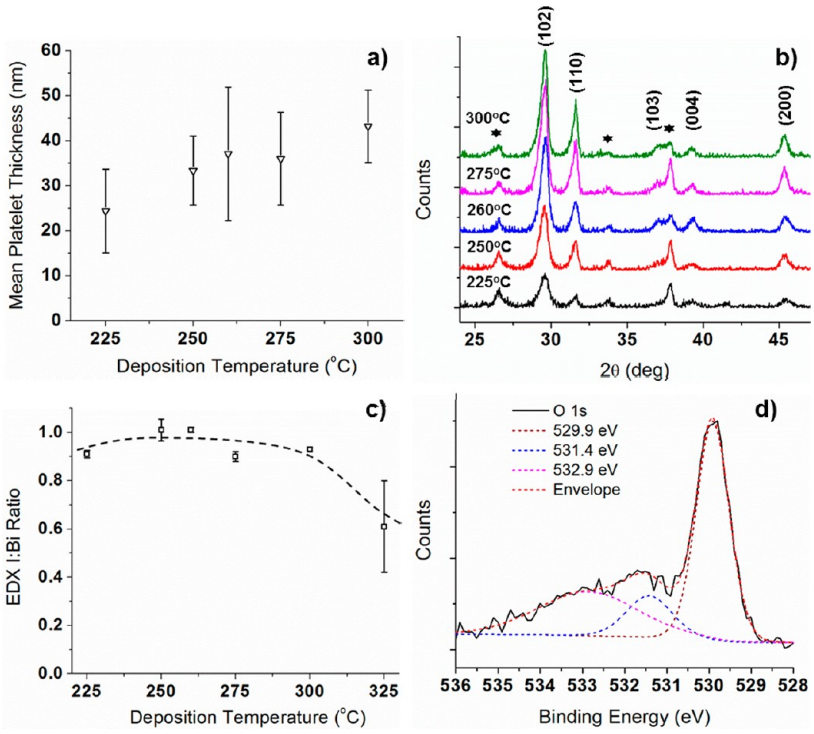

Figure 2. (a) Trend in mean platelet thicknesses measured from SEM images for various deposition temperatures. (b) XRD patterns for films deposited at the indicated temperatures. The indices of the peaks corresponding to BiOI are labeled, and the peaks from the FTO substrate are indicated by *. (c) EDX composition of films deposited at various temperatures. The dashed line is added to guide the eye. (d) Deconvoluted XPS O 1s core-level spectrum obtained for a BiOI film deposited at 260 °C. The position of each fitted peak is indicated in the legend.

O peak area relative to the adsorbate peak areas increased monotonically with deposition temperature from 54% at 250 °C to 65% at 300 °C, indicating that some of these impurities may have been left behind by solution residue that does not completely decompose during deposition. However, part of this impurity signal is likely from the substitution of OH groups for I, resulting in the observed surface I-deficiency. The Bi 4f and I 3d core-level spectra for the BiOI films showed peak positions corresponding to those expected for Bi^{3+} and I^- (see Supporting Information, Figure S-2).[9,22]

Optical Characterization. Optical characterization of films deposited at temperatures between 225 and 300 °C was performed using UV−vis diffuse reflectance measurements. Measured transflectance (transmittance + reflectance) values of both the films and a reference fluorine-doped tin oxide (FTO) substrate were used to calculate absorbance values for each BiOI film (Figure 3a). Qualitatively, the films' light absorption properties changed somewhat with deposition temperature. In particular, a noticeable shoulder was observed at about 640 nm in the spectrum of the film deposited at 225 °C, but this feature diminished as deposition temperature increased, indicating that it is probably an impurity signal from the incomplete decomposition and/or reaction of the precursors. Aside from this feature, the films' qualitative optical properties are similar, although the low coverage of the 300 °C film

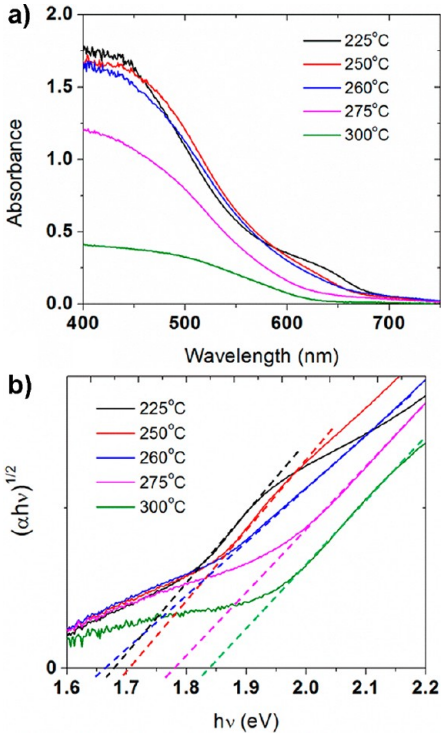

Figure 3. (a) Absorbance spectra of films deposited at various temperatures calculated from UV−vis transflectance measurements in an integrating sphere. (b) Tauc plots created for the absorbance values above, with linear extrapolations to $(\alpha h\nu)^{1/2} = 0$.

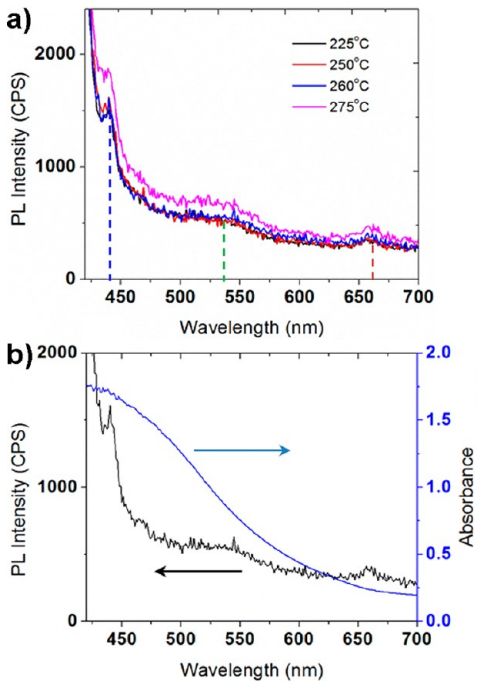

Figure 4. (a) Typical photoluminescence emission spectra of BiOI films deposited at various temperatures on glass with dotted lines indicating the observed peak positions. The excitation wavelength was 400 nm. (b) Photoluminescence emission spectrum (λ_{exc} = 400 nm) and absorbance spectrum of a film deposited at 260 °C.

resulted in significantly lower absorbance values across all wavelengths. When Tauc plots of $(\alpha h\nu)^{1/2}$ *vs* photon energy were generated from the absorbance spectra, the films' indirect band gaps were seen to increase from about 1.7 to 1.8 eV over the given deposition temperature range (Figure 3b). This increase in the apparent band gap probably originates from the removal of impurity states near the band edges. The indirect band gap reported for BiOI typically lies between 1.7 and 1.9 eV,[5,7,8,16] and the ability of BiOI to absorb a large fraction of the visible spectrum is clearly one of its most interesting features as a prospective photocatalyst.

Room-temperature photoluminescence (PL) emission spectra were measured for films deposited on glass substrates at temperatures ranging from 225 to 275 °C (Figure 4). An excitation wavelength of 400 nm was employed for convenient comparison with previous studies.[13,20] Films deposited at 300 °C were not studied since their low coverage led to interference from the relatively more fluorescent glass substrate. The studied films were only very weakly fluorescent, indicating that at room temperature the primary means of recombination are nonradiative, which is typical of indirect band gap semiconductors.[23] All films showed similar emission spectra with three primary features: a sharp peak at 440 nm and two broader peaks at 530 and 660 nm, respectively. Although there is little information regarding the PL spectra of BiOI in the literature, the peak at 440 nm has been assigned to electron and hole recombination across the direct band gap of BiOI, which must therefore lie at approximately 2.8 eV.[20] The other peaks have not yet been identified for BiOI, although defects such as oxygen vacancies have been implicated as sources of broad sub-band-gap PL emission from Bi_2O_3 nanostructures due to carrier trapping and recombination at these states.[24] Similarly, anionic vacancies are expected in these films due to their exhibiting n-type behavior, as discussed below, and the two broader peaks may originate from these vacancies. In general the PL emission spectra are quantitatively quite similar to one another, although the emission intensity of the films deposited at 275 °C was slightly higher than the others. This could indicate that recombination proceeds more quickly in these films than in others, or the difference could simply be due to an increase in the radiative recombination rate relative to nonradiative recombination as a result of increasing vacancy concentrations.

Photoelectrochemical Properties. The PEC performances of films deposited at different temperatures were tested in 0.25 M NaI/acetonitrile. In these experiments I^- acted as a hole scavenger, minimizing the influence of slow charge transfer kinetics to the solution and allowing the bulk charge separation and transport within the films to be analyzed more directly. PEC performance was assessed using both incident photon conversion efficiency (IPCE) calculations under monochromatic illumination and linear sweep voltammetry (LSV) under 100 mW/cm^2 illumination from a solar simulator. In all cases clear cathodic shifts in open circuit potential under illumination and anodic photocurrents were observed, indicating that these films were n-type, which is surprising given the fact that BiOI formed by the anodization of bismuth films in KI electrolyte was reported to be p-type in the earliest study of the PEC properties of BiOI.[17] We observed n-type behavior in both aqueous and nonaqueous solutions and for a number of different electrolyte species, indicating this is not an artifact of solution choice.

To our knowledge, this is the first claim of n-type conductivity put forth for BiOI in the literature. All recent studies employing particulate BiOI photocatalysts appear to have assumed, based on the original thin film study, that BiOI particles are p-type, despite the fact that a few of these recent studies show anodic photocurrents generated by films consisting of BiOI particles.[11,12] Clearly, the common assumption of p-type conductivity in BiOI is not necessarily correct in light of the present results, which suggests that synthesis method may affect the majority carrier type of BiOI. The origin of n-type conductivity in the present films most likely arises from the formation of anion (I^- or O^{2-}) vacancies, which are probably formed due

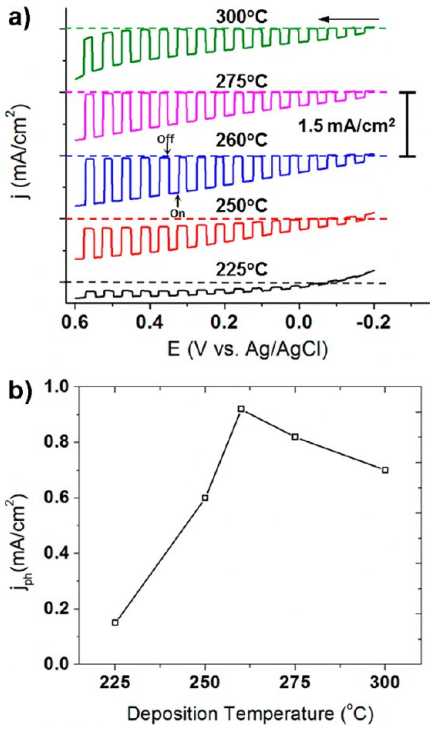

Figure 5. (a) LSV behavior in 0.25 M NaI/acetonitrile for BiOI films deposited at the indicated temperatures. The dashed lines indicate the zero current axes for the plots. The anodic scan rate employed was 25 mV/s. (b) Photocurrent values measured at 0.4 V *vs* Ag/AgCl for these films.

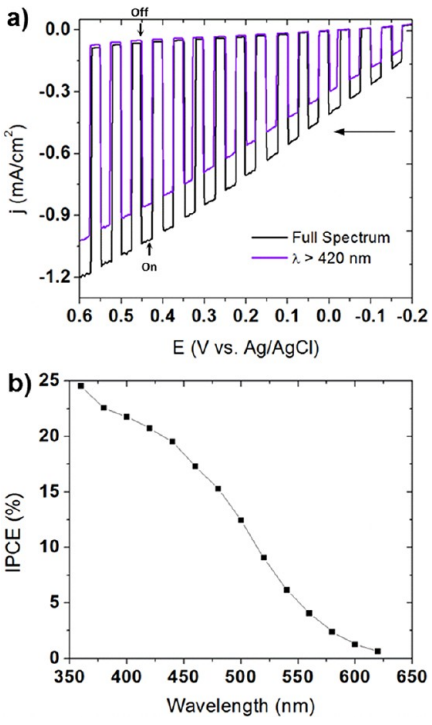

Figure 6. (a) LSV plot using a three-electrode configuration in 0.25 M NaI/acetonitrile both with and without a 420 nm cut-on filter for an optimized film deposited at 260 °C. The anodic scan rate was 25 mV/s. (b) IPCE spectrum recorded at 0.4 V *vs* Ag/AgCl for a typical film deposited at 260 °C with a peak light intensity of 476 μW/cm^2.

to the elevated synthesis temperatures relative to those employed for the anodic synthesis of p-BiOI.[17] EDX analyses indicated that the films were deficient in both oxygen and iodine, although precise quantification, especially of light elements, is difficult employing EDX. Typical LSVs in NaI/acetonitrile under intermittent illumination for films deposited at various temperatures are displayed in Figure 5a. In general, films deposited at higher temperatures (260−300 °C) showed smaller dark currents and larger photocurrents. Films deposited at 260 °C typically showed the highest photocurrents, reaching 0.9 mA/cm^2 at 0.4 V *vs* Ag/AgCl, which is over 20 times higher than the photocurrent density observed for p-BiOI films deposited by anodization (Figure 5b).[17] Films deposited in this temperature range also showed a photocurrent onset at approximately −0.35 V *vs* Ag/AgCl, whereas the onset of significant dark current occurred near 0.5 V. For lower deposition temperatures, the films exhibited relatively high dark currents over a wide potential range, which may be caused by the higher impurity concentration suggested by the optical absorbance spectra. Although the removal of impurities and the improvement in crystallinity would be expected to improve PEC performance at even higher temperatures, these properties may be offset by the decreased light absorption and higher anion vacancy concentrations.

When a filter was employed to remove UV light (λ < 420 nm), the photocurrents remained roughly 75% of those measured under full spectrum illumination for all the films, revealing their excellent PEC activity in the visible range (Figure 6a). The ability of a photocatalyst or photoelectrode to respond to visible light effectively is very important for solar utilization. In this respect these n-BiOI films outperformed other nanostructured photoanodes, such as those composed of TaON or α-Fe_2O_3 nanotubes, which yielded visible-light photocurrent fractions of 47% and 50%, respectively, in an earlier work.[25]

IPCE data measured at 0.4 V *vs* Ag/AgCl in NaI/acetonitrile confirmed the strong spectral response of these films for wavelengths greater than 420 nm. IPCEs for a typical film deposited at 260 °C are displayed in Figure 6b, showing reasonably high conversion efficiencies of up to 25% at 360 nm. The IPCE values decreased significantly above 500 nm and became negligible (<1%) above 620 nm. When the IPCE values were integrated over the AM1.5G solar spectrum,[26] an overall photocurrent of 1.45 mA/cm^2 was calculated. However, the measured photocurrents for these films under simulated AM1.5G illumination are approximately 1 mA/cm^2, suggesting that the photoconversion efficiency was light intensity dependent. Indeed, when the light intensity was decreased from 100 mW/cm^2 to 67 and then 50 mW/cm^2, a sublinear power law

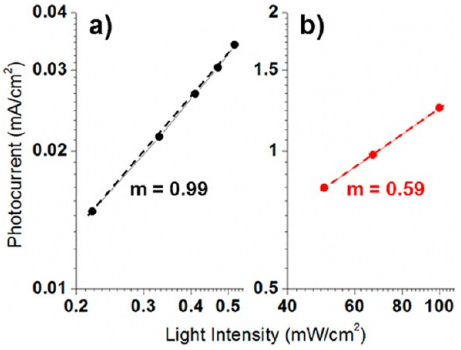

Figure 7. Log−log plots of photocurrent *vs* light intensity at 0.4 V *vs* Ag/AgCl for a film deposited at 260 °C in the low (a) and high (b) light intensity regimes. The slopes of the resulting plots are indicated.

dependence between the photocurrent and light intensity ($J \propto I^{0.59}$) became apparent, in contrast with the linear dependence observed under low-intensity monochromatic (λ = 460 nm) illumination (Figure 7).

Deviation from linear photocurrent *vs* intensity behavior could be caused by several factors such as the direct recombination of conduction band electrons with valence band holes in the space charge region (Langevin recombination) or by surface defects.[27,28] As an example of the latter case, Parkinson *et al*. observed a pronounced sublinear dependence for single crystals of the layered compounds n-WS_2 and n-MoS_2 containing many surface steps. Crystals with well-cleaved surfaces, on the other hand, showed linear photocurrent *vs* intensity response even at high intensities, suggesting that surface states can play a significant role.[28] White *et al*. also observed an influence of unpassivated surface states on the light intensity dependence of another layered compound, n-WSe_2.[29] Their results suggested that exposed non-van der Waals faces (surface states) could facilitate the transfer of conduction band electrons to oxidation reaction products such as I_3^-, which are present at higher concentrations when high light intensities are employed. This is a very reasonable explanation for the observations in the present study since these films expose many such non-van der Waals surfaces.

I−*V* behavior was also measured using a two-electrode configuration and the I^-/I_3^- redox couple (see Supporting Information, Figure S-3). Short circuit current densities of ~0.48 mA/cm^2 were attained under AM1.5G illumination, which are twice as high as those measured in a previous study on BiOI nanoflake solar cells.[14] However, the open circuit voltage we observed is lower than that reported in the previous study (0.45 *vs* 0.62 V). Further optimization of PEC cell geometry and electrolyte may afford further improvements in these properties.

Electrochemical Impedance Spectroscopy. Further investigation of films deposited at various temperatures was accomplished using electrochemical impedance

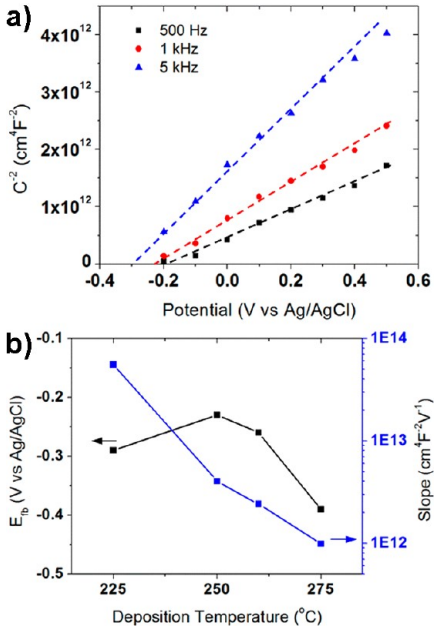

Figure 8. (a) Mott−Schottky plots measured in 0.5 M NaI/0.05 M I_2 in acetonitrile for a film deposited at 260 °C. (b) Derived Mott−Schottky plot parameters at a frequency of 1 kHz displayed as a function of deposition temperature.

spectroscopy (EIS) in a solution of 0.5 M NaI and 0.05 M I_2 in acetonitrile. Impedance data was collected over a range of potentials between −0.2 and 0.5 V *vs* Ag/AgCl, and the results for frequencies between 0.5 and 5 kHz were fitted by an *RC* circuit to generate Mott−Schottky plots of C_{sc}^{-2} *vs* potential, where C_{sc} is the space charge capacitance of the semiconductor electrode. The slopes and *x*-intercepts of such plots are often used to estimate the donor density (N_d) and flat-band potential (E_{fb}) of semiconductor films. Although these particular films are not ideal for Mott−Schottky analysis due to their nanostructured, polycrystalline nature, restricting the frequencies of measurement to moderately high values allowed for consistent results to be obtained.

Representative Mott−Schottky plots using different frequencies for a film deposited at 260 °C are shown in Figure 8a, indicating their linear character as well as their frequency dependence caused by the nonideality of the film−solution interface. The flat-band potentials derived from Mott−Schottky plots (frequency = 1 kHz) for films deposited at various temperatures are shown in Figure 8b and range from −0.23 to −0.39 V *vs* Ag/AgCl, which are similar to the photocurrent onset potentials observed during LSV scans. Films deposited at 300 °C did not yield reliable EIS results due to their lack of coverage of the FTO substrate, however. To further corroborate the flat-band potential measurements, open circuit potentials measured under high-intensity (400 mW/cm^2) illumination were measured. Values of approximately −0.3 V *vs* Ag/AgCl were observed for all deposition temperatures (Figure 9),

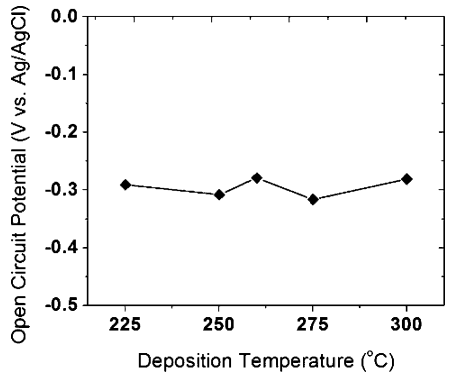

Figure 9. Open circuit potential measurements performed in 0.5 M NaI in acetonitrile under 400 mW/cm^2 illumination for films deposited at various temperatures.

similar to the results of the Mott–Schottky analyses in this solution, and these results indicate that the flat-band potential does not change significantly with deposition temperature.

Another observation that could be made regarding the Mott–Schottky plots is that their slopes decreased consistently as the deposition temperature increased (Figure 8b). This implies that the donor concentration in the films depends on deposition temperature, which would be expected if the electron donors in these films are indeed anion vacancies, the concentration of which would likely be elevated by the higher temperature conditions. The removal of charge-compensating impurities may also result in the apparent increase in donor density, especially between 225 and 250 °C. Differences in electrochemically active surface area could also partly explain some of the differences in the Mott–Schottky slopes, although the growth of larger features at high temperatures should have the opposite effect compared to the observed trend.

Aqueous Electrolyte Behavior. Although good PEC performance was observed in acetonitrile, the PEC activity and stability of BiOI in aqueous solutions are of particular interest for practical application. To assess film activity and stability, BiOI films were tested at various pH's and, at times, with the addition a hole scavenger, SO_3^{2-}. In general, photocurrents measured in aqueous solutions were somewhat lower than those measured in acetonitrile, which seems to have been caused by the reaction of water with the films, particularly at high pH, as discussed below. Markedly different behavior was observed between aqueous 1 M Na_2SO_3 and 1 M $NaSO_4$ solutions at neutral pH (Figure 10). Adding hole scavenger species clearly resulted in much higher photocurrents, particularly at more cathodic potentials, and greatly diminished the transient photocurrent behavior, indicating that charge transfer kinetics were improved. The oxidation of SO_3^{2-} to either SO_4^{2-} or $S_2O_6^{2-}$ is known to be quite thermodynamically favorable, with an initial hole transfer potential of 0.63 V *vs* NHE.[30] Without SO_3^{2-} in the electrolyte the only

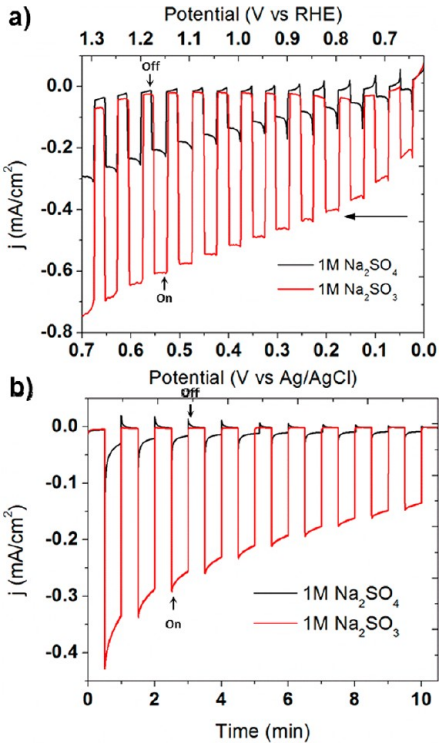

Figure 10. (a) LSVs for BiOI films deposited at 260 °C recorded under intermittent illumination both with and without a hole scavenger species at pH 7. (b) Photocurrent *vs* time plots at a constant potential of 0.5 V *vs* Ag/AgCl in the same solutions.

possible fates of valence band holes in n-BiOI are trapping and recombination with electrons (evidenced by the transient photocurrents), the oxidation of water, or the surface oxidation of BiOI with water (photocorrosion).

Comparing the photocurrent *vs* time behavior of these films in the two solutions revealed that photocorrosion is a major factor in aqueous solutions, especially without a hole scavenger (Figure 10). This indicates that the kinetics of film photocorrosion are more facile than those of water oxidation, which probably results from a lack of overpotential available for water oxidation in the absence of a multielectron transfer catalyst on the surface of BiOI.[31] Without such a catalyst water oxidation probably proceeds *via* the single hole oxidation of H_2O to OH•, which requires an electrochemical potential of 2.73 V *vs* NHE, which is a full 1.5 V more positive than the potential for the four-hole oxidation of H_2O to O_2.[29] The predicted valence band edge of BiOI (roughly 2.4 V *vs* NHE)[11,32] is insufficiently positive to drive this initial charge transfer step efficiently using photogenerated holes. Indeed, a number of studies have suggested that OH• species are not produced on BiOI by valence band holes under illumination in aqueous solutions,[13,16] consistent with the results reported here.

Although the addition of SO_3^{2-} to aqueous solutions impeded photocorrosion to a large extent, it

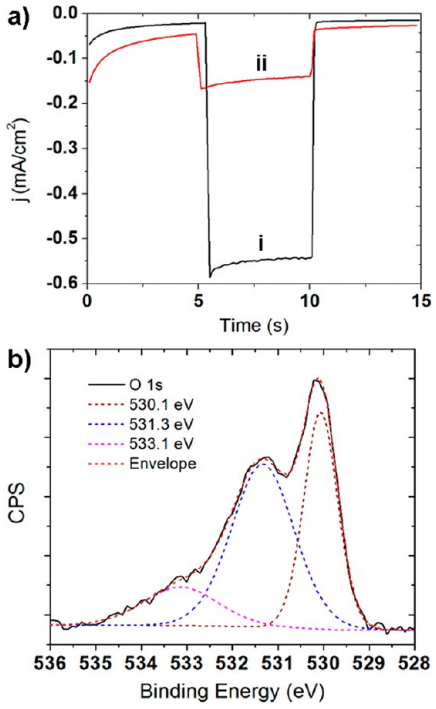

Figure 11. (a) Photocurrent performance at 0.4 V *vs* Ag/AgCl in 1 M Na_2SO_3 of a film deposited at 260 °C measured (i) before and (ii) after 20 min soaking in the dark at pH 7. (b) XPS O 1s spectrum recorded after soaking a film (deposited at 260 °C) in water for several hours.

clearly did not fully suppress the degradation of the PEC activity of n-BiOI, in contrast to the stable behavior observed in acetonitrile solutions containing I^- (see Supporting Information, Figure S-4). Upon further testing, it became clear that even simply immersing the BiOI films in water for an extended period of time led to their deactivation. For example, the photocurrent of a film was measured briefly in 1 M Na_2SO_3, after which it was allowed to soak in this solution in the dark for 20 min. Following this soaking period, the same test was performed, yet the photocurrent was roughly 25% of the initial value (Figure 11a). Similar results were obtained for films soaked in pure water as well.

XPS analyses performed on a film before and after immersion in water for an extended period of time showed substantial differences in the O 1s spectra (Figure 11b), particularly in the pronounced growth of the OH peak at 531.3 eV compared to that observed in Figure 2d. However, no differences existed between XRD patterns for the films before and after soaking. This suggests that only a surface layer of bismuth hydroxide may form on these films upon their exposure to water, which would act as an insulating layer, inhibiting charge transfer. This reaction appeared to be more favorable at higher pH's, as the photocurrents measured in basic solution (pH > 12) were very low. The films appeared to be more stable in acidic electrolytes (pH 1−3) by comparison, but more concentrated acid solutions (pH < 1) led to their fast dissolution. Unfortunately, the chemical instability of BiOI appears to inhibit its use as a photoelectrode in aqueous solutions, despite many reports of its utilization for aqueous photocatalysis. It may be that the surface changes inhibiting the PEC activity in this case have a less drastic effect on the photocatalytic mechanisms typically studied. The coating of a cocatalyst layer, however, may improve both stability and activity in aqueous environments.

CONCLUSIONS

BiOI nanoplatelet films have been synthesized by spray pyrolysis for the first time, and their properties have been studied for various deposition conditions. Deposition temperature affected the platelets' size and crystallographic properties in addition to modifying their chemical composition and optical properties. The films exhibited n-type conductivity, contrary to that commonly reported. Although the origin of n-type conductivity is not definitive, this behavior appears to originate from anion vacancies, as suggested by the compositional analyses and Mott−Schottky results. PEC testing revealed that 260 °C was the optimum substrate temperature during deposition for achieving high anodic photocurrents from the oxidation of I^- to I_3^- in acetonitrile (0.9 mA/cm^2 at 0.4 V *vs* Ag/AgCl under AM1.5G). The films responded well to visible light (~75% photocurrent contribution) and possessed indirect band gaps ranging from 1.7 to 1.8 eV, indicating that n-BiOI films have favorable properties as photoanodes. However, the films showed poor stability in aqueous solutions due to the formation of a surface hydroxide layer, which hindered hole transfer to electrolyte species. The protection of n-BiOI films with a catalyst layer or employing them as a bottom layer in a buried heterojunction scheme may allow their stable use for aqueous photoelectrochemistry.

METHODS

Precursor solutions containing bismuth and iodine were prepared by dissolving $Bi(NO_3)_3 \cdot 5H_2O$ (Alfa) and NH_4I (Acros) in ethylene glycol (99+%, Acros). Ethylene glycol was employed as the solvent in order to dissolve bismuth nitrate and prevent its premature reaction with NH_4I. This precursor solution was loaded into a syringe and pumped through an ultrasonic spray nozzle (130 kHz, Sonotech) positioned above a hot plate in a ventilated enclosure. The spray parameters were controlled by a syringe pump (New Era), which was programmed to spray intermittently (a spray pulse, followed by a rest period) for a set number of deposition cycles. Various nozzle heights and spray parameters were investigated, and those selected for further study were a nozzle height of 12 cm, flow rates between 1.0 and 1.5 mL/min, a pulse volume of 0.3 mL, and a rest time of 25 s. The FTO substrates were mounted on a hot plate using a stainless steel mask, which allowed for a controllable deposition area. Prior to mounting, the substrates were ultrasonically

cleaned with ethanol, rinsed with water, and dried in air. The substrate surface temperature was calibrated for various hot plate settings using an infrared pyrometer (Microepsilon).

SEM and EDX were performed using a Quanta FEG 650 electron microscope (FEI). HRTEM was performed using a JEOL 2010F microscope with an accelerating voltage of 200 kV. XRD experiments utilized a Bruker D8 diffractometer. Mean grain size was calculated using the Scherrer equation:

$$D = \frac{K\lambda}{\beta \cos\theta} \quad (3)$$

Here D is the mean crystallite size, λ is the X-ray wavelength employed (0.154 nm), and β is the full-width at half-max of the diffraction peak of interest. K is a shape factor, typically approximated as 0.9.[33] XPS was performed using a Kratos AXIS X-ray photoelectron spectrometer. The XPS spectra were calibrated to the adventitious carbon peak at 284.5 eV. Total transmittance and diffuse reflectance spectra were measured with a Cary 500 UV−vis−NIR spectrophotometer attached to a Labsphere DRA-CA-5500 integrating sphere. A bare FTO substrate was employed as a baseline standard, and corrected values of transmittance (T) were used to calculate the absorbance (A) using

$$A = -\log_{10}(T) \quad (4)$$

Photoluminescence spectroscopy was performed at room temperature using a Fluorolog-3 spectrofluorometer (Horiba Scientific).

The electrochemical and photoelectrochemical properties of each sample were tested using a three-electrode electrochemical cell with a Ag/AgCl reference electrode and Pt wire counter electrode. All potentials are given relative to Ag/AgCl unless otherwise stated. The working electrode (the photoanode consisting of the BiOI film) with illuminated area 0.21 cm^2 was immersed in the desired electrolyte (typically 0.25 M NaI in acetonitrile) and illuminated by a 150 W solar simulator with an AM1.5G filter (Newport), the overall power density of which was calibrated to 100 mW/cm^2 at the sample surface using a thermopile (Newport). A 420 nm cut-on filter was employed at times to remove UV light. Anodic currents were plotted on the negative axis of the $I-V$ plots. A monochromator (Newport) was employed to study spectral response and was used in conjunction with a monochromatic power meter and photodiode (Newport) to calculate the IPCE from the measured photocurrent density (J_{ph}) and photon flux (I) at a given wavelength (λ) according to

$$\text{IPCE} = \frac{J_{ph}(\lambda)}{I(\lambda)} \times 100\% \quad (5)$$

For each IPCE test, the monochromatic light power incident on the film was calibrated to 100 μW (476 $\mu W/cm^2$) at 460 nm, which was the wavelength of highest intensity. Monochromatic intensities ranged from this value down to 190 $\mu W/cm^2$, depending on the wavelength selected (see Supporting Information, Figure S-5). A potentiostat (CH Instruments, CHI660D) was operated by a desktop computer to perform electrochemical measurements.

Conflict of Interest: The authors declare no competing financial interest.

Acknowledgment. The authors gratefully acknowledge (i) Vincent C. Holmberg for performing UV−vis diffuse reflectance measurements, (ii) the Division of Chemical Sciences, Geosciences, and Biosciences, Office of Basic Energy Sciences, U.S. Department of Energy through Grant DE-FG02-09ER16119, (iii) the Welch Foundation (Grant F-1436) for funding this work, and (iv) a grant (No. 0618242) from the National Science Foundation for funding the X-ray photoelectron spectrometer used for these studies.

Supporting Information Available: Additional XRD patterns, XPS spectra, PEC data, and the monochromator output spectrum, as referenced in the text. This material is available free of charge *via* the Internet at http://pubs.acs.org.

REFERENCES AND NOTES

1. Bard, A. J.; Fox, M. A. Artificial Photosynthesis. *Acc. Chem. Res.* **1995**, *28*, 141–145.
2. Kabra, K.; Chaudhary, R.; Sawhney, R. L. Treatment of Hazardous Organic and Inorganic Compounds through Aqueous-Phase Photocatalysis: A Review. *Ind. Eng. Chem. Res.* **2004**, *43*, 7683–7696.
3. Hashimoto, K.; Irie, H.; Fujishima, A. TiO_2 Photocatalysis: A Historical Overview and Future Prospects. *Jpn. J. Appl. Phys.* **2005**, *44*, 8269–8285.
4. Walter, M. G.; Warren, E. L.; McKone, J. R.; Boettcher, S. W.; Mi, Q.; Santori, E. A.; Lewis, N. S. Solar Water Splitting Cells. *Chem. Rev.* **2010**, *110*, 6446–6473.
5. Lei, Y.; Wang, G.; Song, S.; Fan, W.; Pang, M.; Tang, J.; Zhang, H. Room Temperature, Template-free Synthesis of BiOI Hierarchical Structures: Visible-Light Photocatalytic and Electrochemical Hydrogen Storage Properties. *Dalton Trans.* **2010**, *39*, 3273–3278.
6. Zhang, X.; Zhang, L. Electronic and Band Structure Tuning of Ternary Semiconductor Photocatalysts by Self Doping: The Case of BiOI. *J. Phys. Chem. C* **2010**, *114*, 18198–18206.
7. Zhang, X.; Ai, Z.; Jia, F.; Zhang, L. Generalized One-Pot Synthesis, Characterization, and Photocatalytic Activity of Hierarchical BiOX (X = Cl, Br, I) Nanoplate Microspheres. *J. Phys. Chem. C* **2008**, *112*, 747–753.
8. Chang, X.; Huang, J.; Cheng, C.; Sui, Q.; Sha, W.; Ji, G.; Deng, S.; Yu, G. BiOX (X = Cl, Br, I) Photocatalysts Prepared Using $NaBiO_3$ As the Bi Source: Characterization and Catalytic Performance. *Catal. Commun.* **2010**, *11*, 460–464.
9. Wang, Y.; Deng, K.; Zhang, L. Visible Light Photocatalysis of BiOI and Its Photocatalytic Activity Enhancement by *in Situ* Ionic Liquid Modification. *J. Phys. Chem. C* **2011**, *115*, 14300–14308.
10. Zhang, K. L.; Liu, C. M.; Huang, F. Q.; Zheng, C.; Wang, W. D. Study of the Electronic Structure and Photocatalytic Activity of the BiOCl Photocatalyst. *Appl. Catal. B: Environ.* **2006**, *68*, 125–129.
11. Dai, G.; Yu; Liu, G. Synthesis and Enhanced Visible-Light Photoelectrocatalytic Activity of p−n Junction BiOI/TiO_2 Nanotube Arrays. *J. Phys. Chem. C* **2011**, *115*, 7339–7346.
12. Jiang, J.; Zhang, X.; Sun, P.; Zhang, L. ZnO/BiOI Heterostructures: Photoinduced Charge-Transfer Property and Enhanced Visible-Light Photocatalytic Activity. *J. Phys. Chem. C* **2011**, *115*, 20555–20564.
13. Cheng, H.; Huang, B.; Dai, Y.; Qin, X.; Zhang, X. One-Step Synthesis of the Nanostructured AgI/BiOI Composites with Highly Enhanced Visible-Light Photocatalytic Performances. *Langmuir* **2010**, *26*, 6618–6624.
14. Wang, K.; Jia, F.; Zhi, Z.; Zhang, L. Crossed BiOI Flake Array Solar Cells. *Electrochem. Commun.* **2010**, *12*, 1764–1767.
15. Tributsch, H. Electronic Structure, Coordination Photoelectrochemical Pathways and Quantum Energy Conversion by Layered Transition Metal Dichalcogenides. In *Photoelectrochemistry and Photovoltaics of Layered Semiconductors*; Aruchamy, A., Ed.; Kluwer: Dordrecht, 1992; pp 83−116.
16. Li, Y; Wang, J.; Yao, H.; Dang, L.; Li, Z. Efficient Decomposition of Organic Compounds and Reaction Mechanism with BiOI Photocatalyst Under Visible Light Irradiation. *J. Mol. Catal. A: Chem.* **2011**, *334*, 116–122.
17. Poznyak, S. K.; Kulak, A. I. Photoelectrochemical Properties of Bismuth Oxyhalide Films. *Electrochim. Acta* **1990**, *35*, 1941–1947.
18. Liu, H.; Cao, W.; Sua, Y.; Wanga, Y.; Wang, X. Synthesis, Characterization and Photocatalytic Performance of Novel Visible-Light-induced Ag/BiOI. *Appl. Catal. B: Environ.* **2012**, *111*, 271–279.
19. Xia, J.; Yina, S.; Li, H.; Xu, H.; Xu, L.; Zhang, Q. Enhanced Photocatalytic Activity of Bismuth Oxyiodine (BiOI) Porous Microspheres Synthesized *via* Reactable Ionic Liquid-assisted Solvothermal Method. *Colloid Surf. A* **2011**, *387*, 23–28.
20. Ye, L.; Tian, L.; Peng, T.; Zan, L. Synthesis of Highly Symmetrical BiOI Single-Crystal Nanosheets and Their {001} Facet-Dependent Photoactivity. *J. Mater. Chem.* **2011**, *21*, 12479–12484.

21. Huang, W. L. Electronic Structures and Optical Properties of BiOX (X = F, Cl, Br, I) *via* DFT Calculations. *J. Comput. Chem.* **2009**, *30*, 1882–1891.
22. Zhao, Z.; Liu, F.; Zhao, L.; Yan, S. Preparation and XPS Study of X-ray Photochromic Transparent BiOI/Nylon11 Composite Film. *Appl. Phys. A: Mater. Sci. Process.* **2011**, *103*, 1059–1065.
23. Gfroerer, T. H. Photoluminescence in Analysis of Surfaces and Interfaces. In *Encyclopedia of Analytical Chemistry*; John Wiley and Sons: Chichester, 2000; pp 9209−9231.
24. Kumari, L.; Lin, J. H.; Ma, Y. R. One-Dimensional Bi_2O_3 Nanohooks: Synthesis, Characterization and Optical Properties. *J. Phys.: Condens. Matter* **2007**, *19*, 406204.
25. Banerjee, S.; Mohapatra, S. K.; Misra, M. Synthesis of TaON Nanotube Arrays by Sonoelectrochemical Anodization Followed by Nitridation: a Novel Catalyst for Photoelectrochemical Hydrogen Generation from Water. *Chem. Commun.* **2009**, 7137–7139.
26. NREL AM 1.5 Gobal Solar Spectrum Derived from SMARTS v.2.9.2; http://rredc.nrel.gov/solar/spectra/am1.5/.
27. Chandra, S. Theoretical Models. In *Photoelectrochemical Solar Cells*; OPA: Amsterdam, 1985; pp 193−236.
28. Kline, G.; Kam, K.; Ziegler, R.; Parkinson, B. A. Further Studies of the Photoelectrochemical Properties of the Group VI Transition Metal Dichalcogenides. *Sol. Energ. Mater.* **1982**, *6*, 337–350.
29. White, H. S.; Abruna, H. D.; Bard, A. J. Semiconductor Electrodes. *J. Electrochem. Soc.* **1982**, *129*, 265–271.
30. Wardman, P. Reduction Potentials of One-Electron Couples Involving Free Radicals in Aqueous Solution. *J. Phys. Chem. Ref. Data* **1989**, *18*, 1637–1755.
31. Cowan, A. J.; Barnett, C. J.; Pendlebury, S. R.; Barroso, M.; Sivula, K.; Graetzel, M.; Durrant, J. R.; Klug, D. R. Activation Energies for the Rate-Limiting Step in Water Photooxidation by Nanostructured α-Fe_2O_3 and TiO_2. *J. Am. Chem. Soc.* **2011**, *133*, 10134–10140.
32. Wang, W.; Huang, F.; Lin, X.; Yang, J. Visible-Light-responsive Photocatalysts xBiOBr−(1−x)BiOI. *Catal. Commun.* **2008**, *9*, 8–12.
33. Holzwarth, U.; Gibson, N. The Scherrer Equation *versus* the 'Debye-Scherrer Equation'. *Nat. Nanotechnol.* **2011**, *6*, 534.